

Slow Neutron Inelastic Scattering from Liquid Sodium*

P. D. RANDOLPH

Atomic Energy Division, Phillips Petroleum Company, Idaho Falls, Idaho

(Received 24 September 1963; revised manuscript received 7 February 1964)

Partial differential cross sections for slow neutron scattering from liquid sodium have been measured at 100, 150, and 200°C. The Materials Testing Reactor phased-chopper velocity selector was used with a 95% transmission sample at incident neutron energies of 0.025, 0.07, and 0.10 eV at eight scattering angles (16 to 85°). In the scattering law obtained from these cross sections, prominent coherent scattering maxima appear for energy transfers $\Delta E \leq 0.2 k_B T$, but disappear beyond $\Delta E = 0.3 k_B T$. At each temperature, time-dependent widths $\rho(t)$ of the intermediate scattering function have been obtained by Fourier transformation of the scattering law for large momentum transfers. At times $< 1 \times 10^{-13}$ sec these functions confirm the prediction of gas-like behavior, but at larger times are solid-like. The $\rho(t)$'s are also momentum-dependent at larger times indicating that the self-correlation function is not strictly Gaussian. Measurements of the zeroth and first moments of the energy transfer have been obtained from the scattering law at each temperature for several values of momentum transfer. The zeroth moment is in agreement with neutron diffraction experiments, but the first moment is as much as a factor of 2.5 larger than predicted theoretically.

I. INTRODUCTION

THIS report gives the results of an experimental measurement of the partial differential cross sections for slow neutron scattering by liquid sodium. Besides the cross sections themselves, which are of interest to reactor technology, information about the dynamics of the motions of atoms in the liquid can be obtained from them. Extensive investigations of this type have been made for water^{1,2} and for liquid lead.³ Sodium was chosen as the sample for this experiment because it meets the following requirements: (A) The liquid is monatomic so that no molecular effects occur. (B) The isotopic abundance is 100% Na²³ so that the scattering from only a single isotope is involved. (C) It is one of the few elements meeting the first two requirements whose incoherent scattering cross section (1.85 b) is a large fraction of the total scattering cross section (3.4 b), and which also has a reasonably low absorption cross section (0.5 b). A relatively large incoherent cross section is desirable since it is only the incoherent scattering which yields information about the motions of individual atoms. A cold-neutron study of sodium has been made by Cocking⁴ who studied the inelastic scattering in the range 80 to 200°C.

The present experiment was performed using the Materials Testing Reactor (MTR) slow-neutron phased-chopper velocity selector at incident neutron energies of 0.025, 0.07, and 0.10 eV at sample temperatures of 100, 150, and 200°C. The experimental data show that

marked inelastic interference scattering occurs up to energy transfers $\Delta E \approx 0.2 k_B T$. Time-dependent width functions obtained from the data show that the self-part of the space-time correlation function is fitted well by the Gaussian approximation at very short time, but at intermediate times, Gaussian width functions differ by as much as a factor of 2 for different momentum transfers. We have also measured the first energy transfer moment of the scattering law at several fixed values of momentum transfer including corrections for multiple scattering and find that these are as much as a factor of 2.5 larger than predicted.

II. EXPERIMENTAL PROCEDURE

The MTR 4-rotor phased-chopper velocity selector used in this experiment has been described elsewhere in detail.⁵ This velocity selector produces bursts of nearly monochromatic neutrons of thermal energies by the use of two Fermi choppers spinning at the same speed (5000 rpm) and phased with each other. The scattering target is placed 0.5 m beyond the second chopper and the scattered neutrons are detected simultaneously at eight scattering angles by BF₃ counter banks located 2 m from the sample. These detectors were at scattering angles of 16.3, 20.1, 26.0, 36.4, 47.6, 59.5, 72.1, and 84.7°, and subtended 7.5° in the scattering plane except the detector at 20.1° which subtended 3.5°.

The energy, flux, and time resolution of the incident neutrons are determined by a U²³⁵ fission chamber located in the transmitted beam 2 m from the sample. For each data run at a given temperature, the sample and empty sample are cycled alternately into the beam at 10-min intervals for a total running time of 48 h or longer. The data from each of the two holders are stored in a separate matrix of the 8192 channel time-of-flight analyzer. For this experiment, 256 10-μsec channels were used to time-analyze the data for each

* Work performed under the auspices of the U. S. Atomic Energy Commission.

¹ M. Sakamoto, B. N. Brockhouse, R. G. Johnson, N. K. Pope, *J. Phys. Soc. Japan Suppl. BII*, 370 (1962).

² K. E. Larson, N. Dahlberg, *Proceedings of the Chalk River Symposium on Inelastic Scattering of Neutrons in Solids and Liquids* (International Atomic Energy Association, Vienna (1963), Vol. 1, p. 317).

³ B. N. Brockhouse, N. K. Pope, *Phys. Rev. Letters* **3**, 259 (1959).

⁴ S. J. Cocking, *Proceedings of the Chalk River Symposium on Inelastic Scattering of Neutrons in Solids and Liquids* (International Atomic Energy Agency, Vienna, 1963), Vol. 1, p. 227.

⁵ R. M. Brugger, J. E. Evans, *Nucl. Instr. Methods* **12**, 75 (1961).

angle and also for the beam monitor. Background corrections are made by subtracting the empty-holder data from the filled sample-holder data. If necessary, these data are normalized to the same counting rate at long and short flight times. After corrections for

detector efficiency, the data are then converted to cross section and scattering law. The data of this experiment comprise runs made at 100, 150, and 200°C at each of the incident energies of 0.025, 0.07, and 0.10 eV. The runs at 100 and 150°C were taken at the 8

FIG. 1. Partial differential cross sections for scattering 0.0249 eV neutrons from liquid sodium at 100°C.

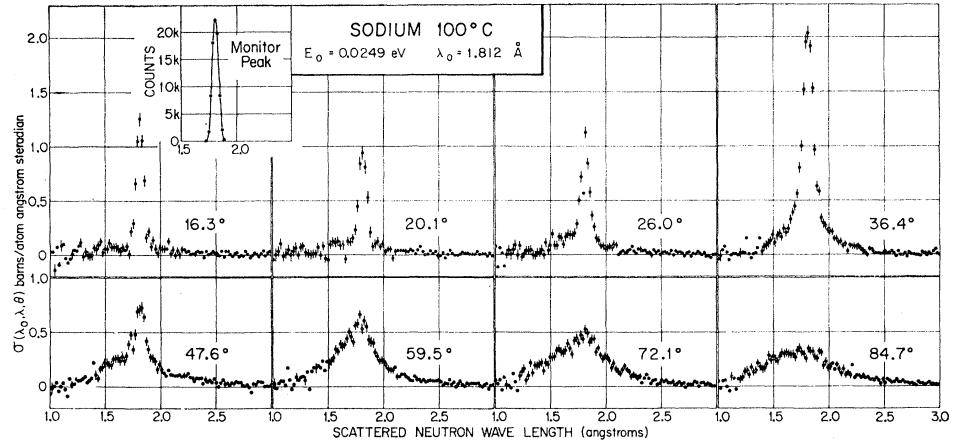


FIG. 2. Partial differential cross sections for scattering 0.0248 eV neutrons from liquid sodium at 150°C.

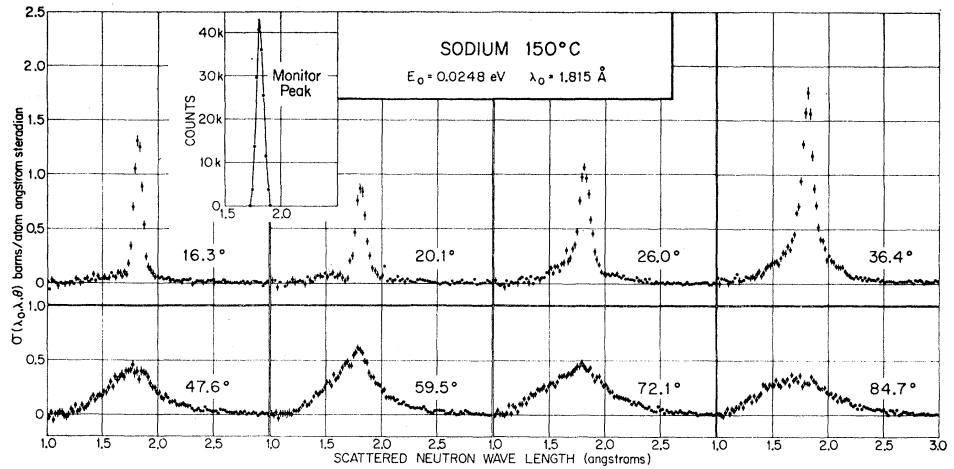
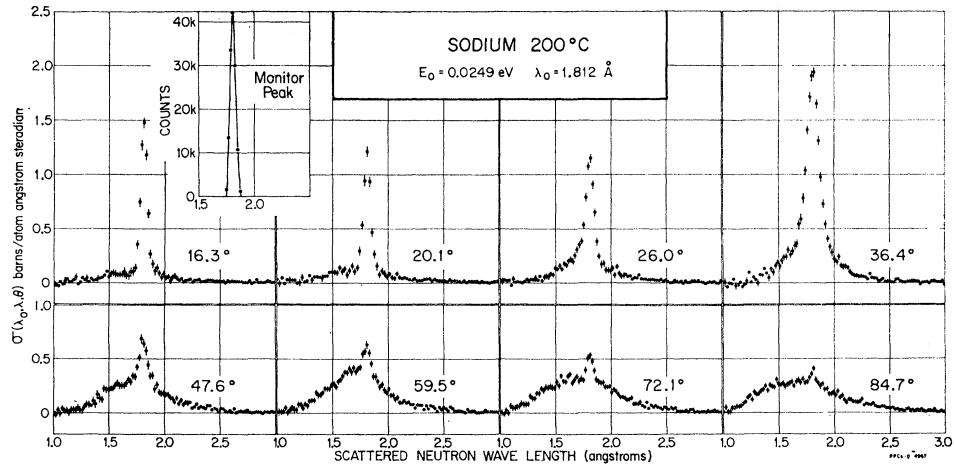


FIG. 3. Partial differential cross sections for scattering 0.0249 eV neutrons from liquid sodium at 200°C.



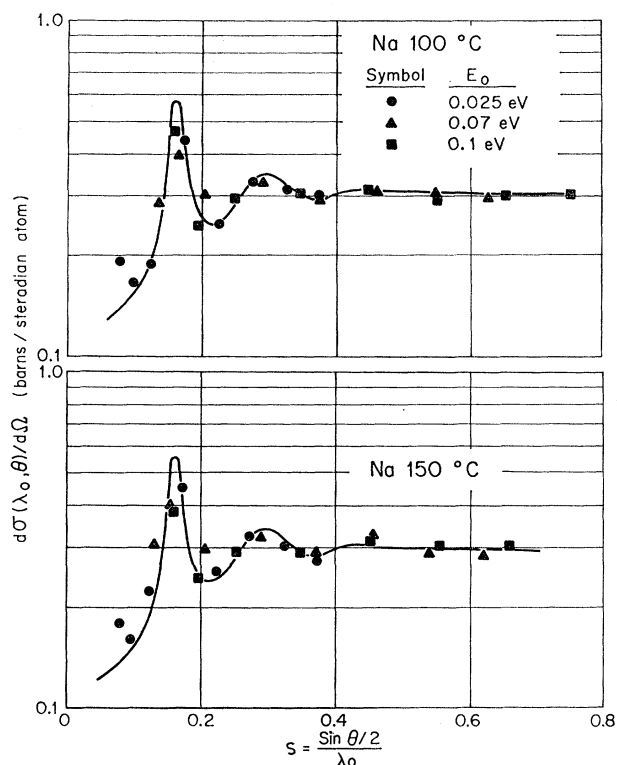


FIG. 4. Diffraction pattern for liquid sodium. The solid curve at both temperatures is the crystal spectrometer result at 100°C of Gingrich and Heaton (Ref. 7).

angles mentioned. At 200°C, additional detector angles of 84.4, 96, 107, 120, and 133° were used with a chopper speed of 6000 rpm.

The liquid-sodium sample used in this experiment was in the form of a rectangular slab having a thickness of 0.25 in. It was made as thin as possible in order to reduce effects of multiple scattering, and the above thickness is a compromise between this criterion and reasonable counting rates. The calculated transmission for thermal neutrons incident normally on the slab is 95%. In practice, the sample was oriented at 45° to the incident beam and was viewed in transmission by the detectors so that the effective transmission for this orientation was 91.5%. Multiple scattering in this sample is estimated to be less than 10% of the single scattering.

The sample holder was made of two hardened aluminum frames having a 0.25-in.-thick spacer between them. The frames sandwiched 0.001-in.-thick stainless steel windows against the spacer. The total window area of the holder was $5\frac{1}{2} \times 3$ in. Gasketing was accomplished by a narrow metal-to-metal contact around the edges of the window. No evidence of any leakage occurred at any time during the experiment. The difference in the thermal expansion coefficients of the aluminum and stainless steel kept the windows taut and no evidence of bulging of the sample was seen. The holder was made

TABLE I. Velocity selector energy resolution for elastic scattering.

Temp.	E_0 (eV)	Δt (μ sec)	$\Delta t/t$	$\Delta E/E_0$	$\Delta\beta$
100°C	0.025	36	0.0393	0.079	0.031
	0.07	36	0.0658	0.132	0.144
	0.10	36	0.0786	0.157	0.245
150°C	0.025	37.5	0.0410	0.082	0.028
	0.07	35	0.0143	0.129	0.124
	0.10	33.5	0.0735	0.147	0.201
200°C	0.025	31	0.0323	0.0645	0.020
	0.07	29.5	0.0567	0.113	0.097
	0.10	30	0.0657	0.131	0.160

taller than needed and was filled to less than capacity to allow for expansion of the sodium on melting. This further reduced any chance of bulging. The holder was not sealed from the atmosphere and in order to prevent excessive oxidation, it was operated under an argon purge. The purge volume was above the top of the beam so that there was no scattering from the argon. The window area was made large enough to accommodate the entire beam area (4×1.30 in.) and the frame was covered with cadmium to reduce the possibility of secondary scattering from the frame. Both the filled and empty holders were heated by 150-W cartridge heaters inserted into the top and bottom edges of each sample holder frame. The temperature was controlled automatically using a chromel-alumel thermocouple located at the edge of the spacer frame. After completion of the experiment, the sample holder was disassembled and the sodium sample analyzed. Spectrographic analysis showed only traces of Al, Ca, Cu, Fe, Mg, and Si. X-ray reflection patterns showed a thin film ($\sim 100 \mu$) of NaOH and NaO on the surfaces. The NaOH is believed not to have been present during the experiment but was formed afterward due to H_2O contamination of the kerosene used to store the disassembled sample.

III. EXPERIMENTAL RESULTS

Typical partial differential cross sections for liquid sodium are shown in Figs. 1–3 for an E_0 of 0.025 eV at each of the three temperatures. The counting rate data used for these figures were not smoothed. The “five-point data smoothing” technique⁶ previously used, although it works very well for gases, is not satisfactory for sodium because the narrow quasielastic peaks (especially at forward angles) are comparable in width to the number of channels used to smooth the data. The result is that the smoothing gives counting rates that are too low (or even negative) at the base of the peak where the slope is changing rapidly. The error flags shown in the figures are counting statistics only. The 150 and 200°C data are of somewhat better quality than that at 100°C since the run times for these

⁶ P. D. Randolph, R. M. Brugger, K. A. Strong, R. E. Schmunk, Phys. Rev. 124, 460 (1961).

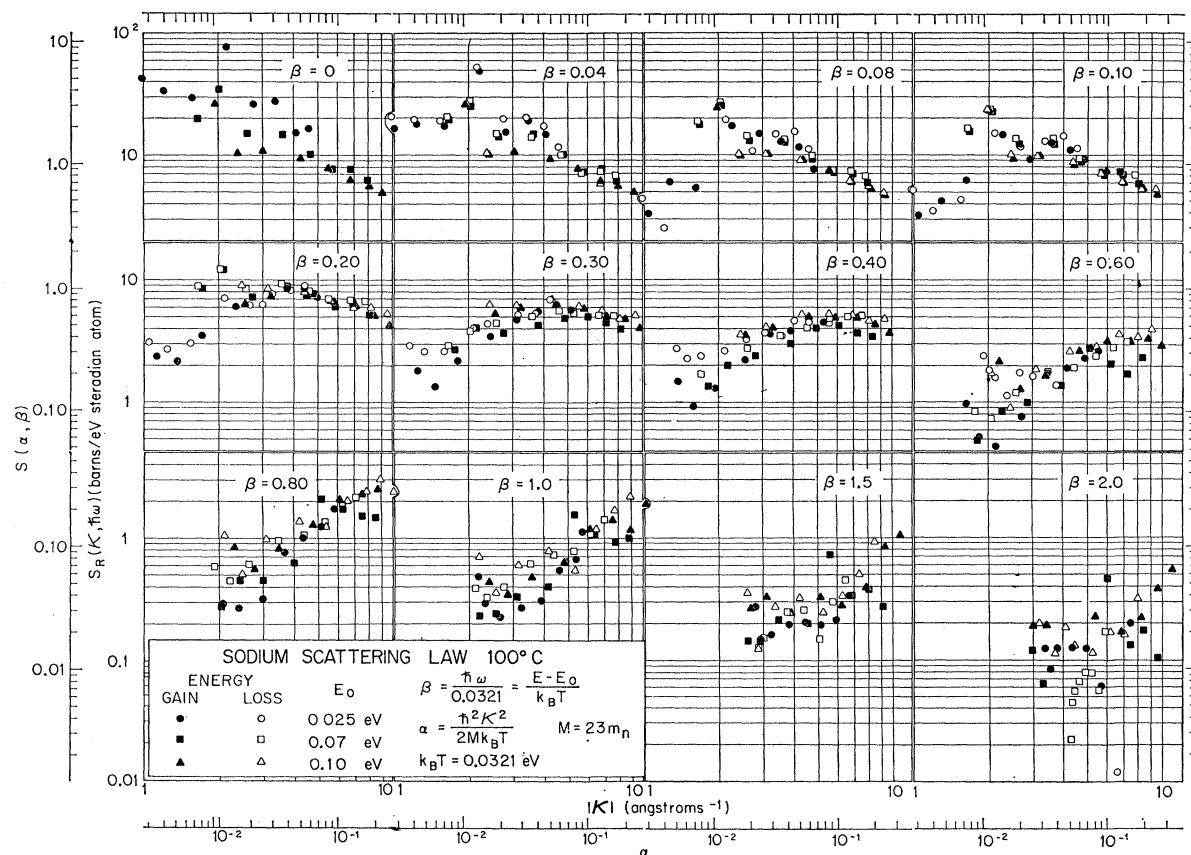


Fig. 5. Reduced partial differential cross sections for sodium at 100°C.

were each of 64 h, whereas the 100°C data were run only for 48 h.

A measure of the energy resolution for elastic scattering is given by the burst shapes of the incident beam which are also shown in the figures. Table I gives a summary of the widths of the bursts Δt (full width at half-maximum) measured by the beam monitor 2 m from the sample. This is calculated by $\Delta t/t_0$ where t_0 is the sample-to-detector time-of-flight at the incident energy E_0 and $\Delta E/E_0 = 2(\Delta t/t_0)$. The resolution is also expressed in terms of $\Delta\beta = \Delta E/2k_B T$, where T is the sample temperature.

The improvement in resolution at 200°C is due to the higher chopper speed (6000 rpm) used at this temperature.

The spectra for each temperature show two general features, a narrow quasielastic peak and a low broad spectrum of inelastically scattered neutrons. At the three forward angles, where the momentum transfers are small, the quasielastic scattering dominates and the inelastic scattering is very small. At 36°, the quasielastic peak is quite large compared with the other angles and the inelastic scattering has become larger. The momentum transfer for this quasielastic peak corresponds to the first maximum in the diffraction pattern

so that this peak has a large contribution from coherent scattering. As the scattering angle continues to increase, the quasielastic peak becomes small or disappears and the inelastic scattering dominates the spectrum. The fact that at 200°C a quasielastic peak is seen at all angles is probably due to the improved resolution used at this temperature. Except for this, the spectra at each angle are qualitatively the same, and only small quantitative differences in the inelastic spectrum are present. At the 0.07 and 0.1 eV incident energies which are not shown, the data cannot be easily resolved into a quasielastic and an inelastic part. The cross sections shown in these figures are normalized to the total cross section value of 3.4 b.

Figure 4 shows the diffraction pattern obtained at 100 and 150°C by integrating the observed cross sections over the scattered wavelength. These are plotted as $d\sigma(\lambda_0)/d\Omega$ versus $s = \sin^2\theta/\lambda_0$, and each plot includes the data from each of the three incident energies. The solid curve is the 100°C result of Gingrich and Heaton⁷ obtained using a neutron crystal spectrometer and is normalized to the data at large s . The agreement is good except at the smaller values of s , where the finite

⁷ N. S. Gingrich, L. Heaton, J. Chem. Phys. **34**, 873 (1961).

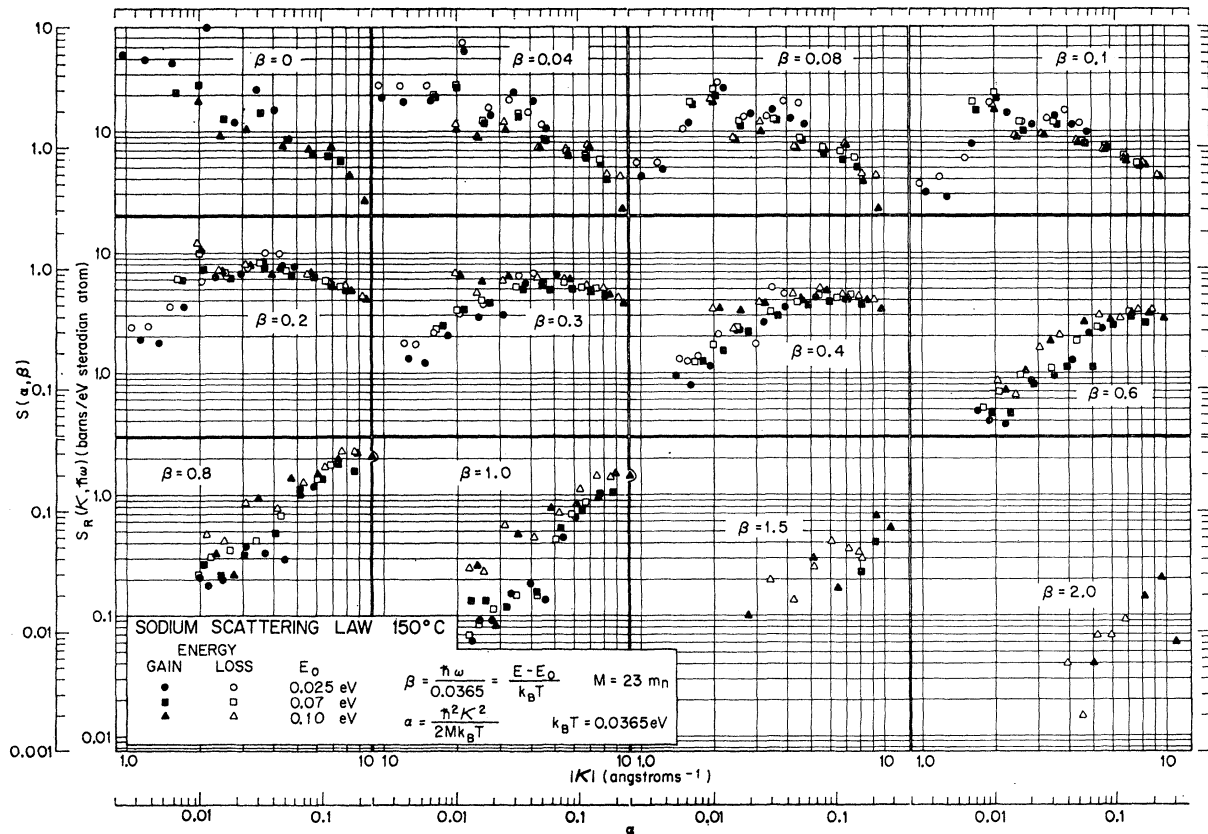


FIG. 6. Reduced partial differential cross sections for sodium at 150°C.

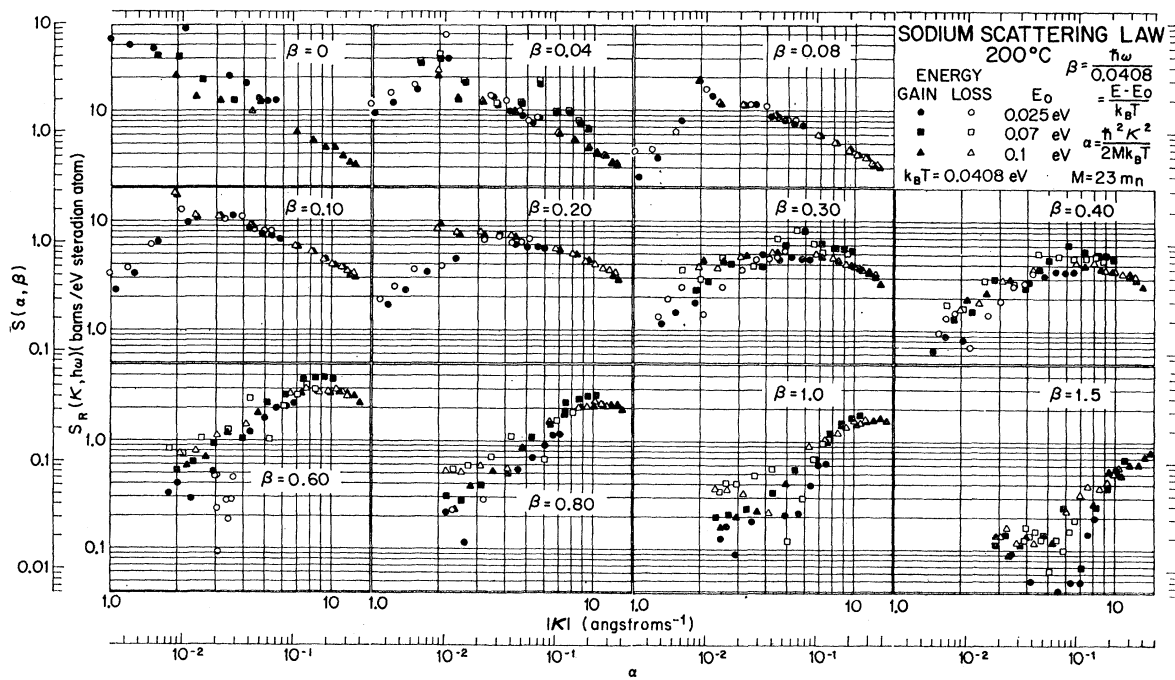


FIG. 7. Reduced partial differential cross sections for sodium at 200°C.

angular resolution of the detectors becomes important. The two major diffraction maxima are clearly evident.

The complete presentation of all the data is given in Figs. 5-7 in terms of the scattering law. This form is used since it is representative of all the data and is a very compact form. The form of the scattering law used is the "reduced partial differential cross section"⁸ $S_R(|\kappa|, \hbar\omega)$ and is defined by

$$d^2\sigma(E_0, E, \theta)/dE d\Omega = [E/E_0]^{1/2} \exp[-\hbar\omega/2k_B T] S_R(\kappa, \hbar\omega), \quad (1)$$

where

$$\begin{aligned} \hbar\omega &= E - E_0, \\ \kappa &= \mathbf{k} - \mathbf{k}_0, \end{aligned}$$

where E_0 , E , \mathbf{k}_0 , and \mathbf{k} are the energy and reduced wave vectors of the incident and scattered neutron, respectively, and θ is the scattering angle. This form obeys the conditions of detailed balance and is even in the energy transfer and in the magnitude of the momentum transfer. The results at each temperature are plotted as S_R versus κ for fixed values of $\hbar\omega$ (in units of $k_B T$). This form has the dimensions of a cross section (b/eV sr atom) and is related to the dimensionless form⁹ of the scattering law $S(\alpha, \beta)$ by

$$S_R(\kappa, \hbar\omega) = (\sigma_b/4\pi k_B T) S(\alpha, \beta), \quad (2)$$

where

$$\begin{aligned} \alpha &= \hbar^2 \kappa^2 / 2M k_B T, \\ \beta &= \hbar\omega / k_B T. \end{aligned}$$

The mass of the scattering atom is given by M , T is the absolute temperature of the sample, and σ_b is the bound-atom cross section. Scales for $S(\alpha, \beta)$ are also shown in the figures.

The range of momentum transfers spanned at each incident energy overlap so that in these regions, the scattering law is overdetermined. At any fixed incident energy, the smallest scattering angle has the smallest κ value. At low-energy transfer ($\beta \lesssim 0.1$) the effects of finite energy resolution cause the data from the different incident energies to form separate curves at the smaller angles, the higher energy curves being below the lower. At larger angles where resolution effects are small, the different incident energies give a single curve. In spite of the energy resolution, the effects of interference scattering are clearly present. The interference maxima are seen, corresponding to those seen in Fig. 4. These maxima are present at each temperature out to energy transfer $\hbar\omega \lesssim 0.25 k_B T$, and disappear beyond this. This fact demonstrates that in sodium, the convolution approximation¹⁰ is not adequate for energy transfers larger than about $0.25 k_B T$ since it predicts contributions

⁸ R. M. Brugger, Atomic Energy Commission Research and Development Report No. IDO-16694 (Rev) 1962 (unpublished).

⁹ P. A. Egelstaff, *Proceedings of the Vienna Symposium on Inelastic Scattering of Neutrons in Solids and Liquids* (International Atomic Energy Agency, Vienna 1961), p. 25.

¹⁰ G. H. Vineyard, *Phys. Rev.* **110**, 999 (1958).

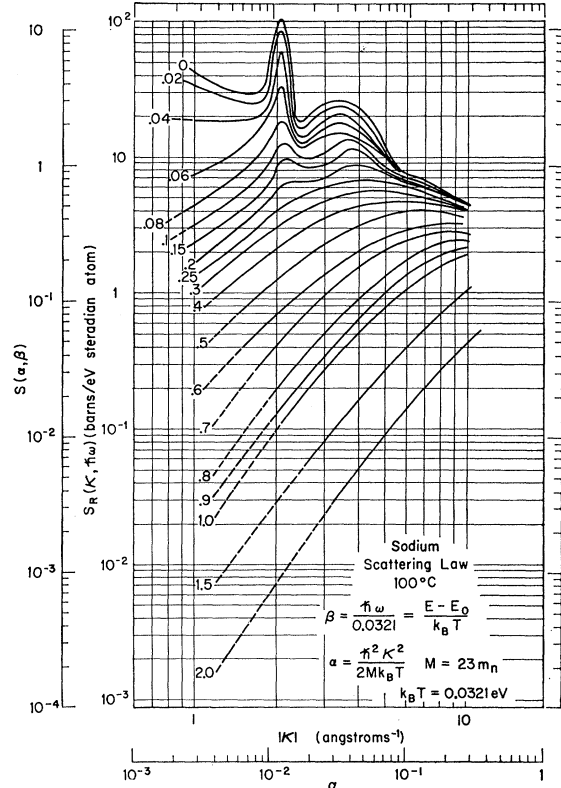


FIG. 8. Smooth curve scattering law for sodium at 100°C.

to the coherent scattering that have magnitudes which are independent of the energy transfer. For small energy transfers at low-momentum transfers, however, cold-neutron results⁴ show that the convolution approximation is in agreement with the experiment.

Smooth-curve scattering laws were obtained for each temperature by making a hand-drawn fit to the data. These are shown in Figs. 8-10. They are plotted as reduced partial differential cross sections $S_R(\kappa, \hbar\omega)$. Also shown are scales for the Egelstaff scattering law $S(\alpha, \beta)$. In drawing these, an attempt was made to reduce the effects of energy resolution by drawing the curve at low κ values for $\beta < 0.3$ to follow or lie above the lowest incident energy data.¹¹ Qualitatively, these curves are quite similar at each of the three temperatures indicating that from 100 to 200°C little change occurs in the properties of the liquid. All the smooth $S_R(\kappa, \hbar\omega)$ curves and the data plots are normalized to the total cross section using the value $\sigma = 3.4$ b.

IV. GAUSSIAN WIDTH FUNCTIONS

As was first shown by van Hove,¹² the scattering law is related to a time-dependent pair-correlation function for the system by a double Fourier transformation.

¹¹ R. M. Brugger, *Phys. Rev.* **126**, 29 (1962).

¹² L. van Hove, *Phys. Rev.* **95**, 249 (1954).

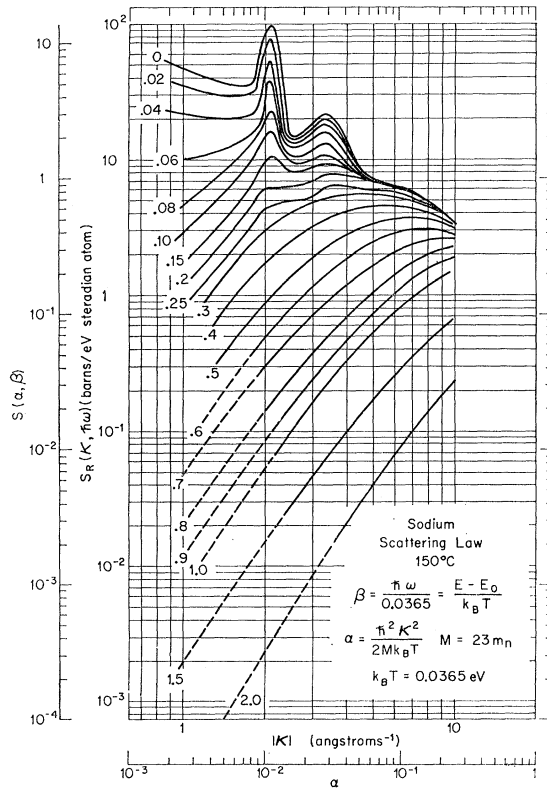


FIG. 9. Smooth curve scattering law for sodium at 150°C.

Various theoretical models for this correlation function have been studied for simple liquids. Vineyard¹⁰ was the first to propose a specific model for the self-part of the correlation function which describes the self-diffusion of the liquid. The model proposed by Vineyard is that the self-part of the space-time correlation function is Gaussian in its space dependence with a time-dependent width. This model was shown to hold for a perfect gas, an oscillator, a Debye lattice, and for an atom obeying the classical equation of diffusion. This model is usually assumed to hold for simple liquids, at least as a first approximation. Indeed, it has been shown by Rahman *et. al.*,¹³ that the Gaussian assumption enters as the first-order term in an expansion of the so-called intermediate scattering function in powers of κ^2 .

In order to find out from experiment how well the Gaussian assumption holds, it is more convenient to work with this intermediate scattering function rather than with the correlation function or the scattering law. Defining a width function $\rho(t)$ by the Gaussian self-correlation function $G_s(r, t)$,

$$G_s(r, t) = [\pi\rho(t)]^{-3/2} \exp[-r^2/\rho(t)] \quad (3)$$

then the intermediate scattering function $I_s(\kappa, t)$, which

¹³ A. Rahman, K. S. Singwi, A. Sjölander, Phys. Rev. **126**, 986 (1962).

is the Fourier transform of G_s over space, may be written as a Fourier transform of the scattering law over the energy transfer.

$$I_s(\kappa, t) = \exp[-\kappa^2\rho(t)/4] = 2 \int_0^\infty \cos(\beta\tau) S_s(\alpha, \beta) d\beta, \quad (4)$$

where in the right-hand member, we have used the symmetric form of the scattering law, and $\tau = (k_B T / \hbar)t$.

The use of the symmetric form of the scattering law implies that $\rho(0) = \hbar^2 / 2Mk_B T$ rather than $\rho(0) = 0$. This constant term is of purely quantum-mechanical origin and is very small. From Eq. (4), if the Gaussian assumptions hold exactly, measurement of $S(\alpha, \beta)$ at fixed α (i.e., fixed κ^2) in principle allows a determination of $\rho(t)$ as was first pointed out by Vineyard.¹⁰ Since $S(\alpha, \beta)$ is known for a range of α , then $\rho(t)$ is overdetermined. If the Gaussian assumption is exact, then the $\rho(t)$ obtained by Fourier transforming S at different values of α should give the same function and, hence, furnishes a test of the assumption.

Fourier transformation of the scattering law for liquid sodium has been performed at each of the three temperatures for several values of α using a program previously written.¹¹ Since it is only the noninterference portion of S that contains information about the diffusive motions, the range of α at which the trans-

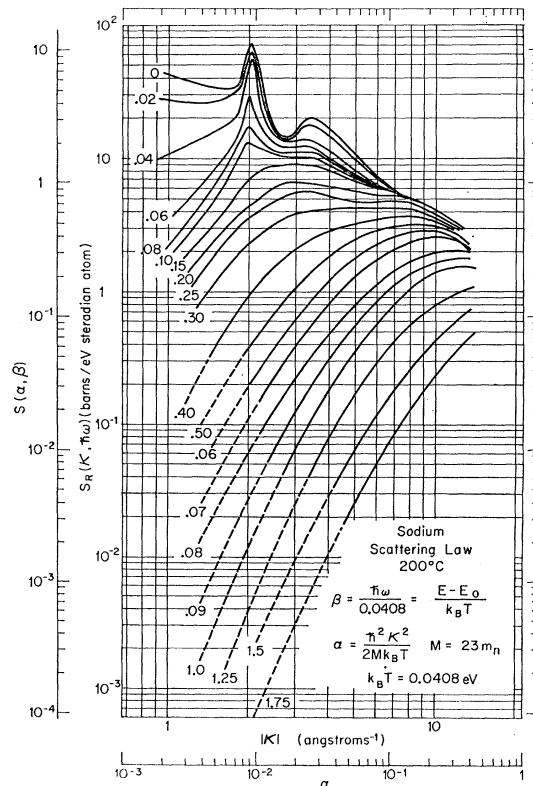


FIG. 10. Smooth curve scattering law for sodium at 200°C.

formation was computed for $\alpha \geq 0.1$ at each temperature using the smooth curve scattering laws shown in Figs. 8-10. It is seen that for $\alpha \gtrsim 0.1$, the strong interference effects have disappeared. The advantage of this region of α space is that no approximate method need be used to separate the interference and the noninterference parts of the scattering. The disadvantage of this is that Fourier transformation at large α restricts the range for which $\rho(t)$ can be obtained to relatively short times. In making these transformations, $S(\alpha, \beta)$ was assumed to go linearly to zero beyond $\beta = 2$. In all cases, this gave a zero value for $S(\alpha, \beta)$ at $\beta \leq 2.4$.

Figure 11 shows the resulting width functions plotted as a function of time for various fixed values of α . Also, there is shown for comparison, the slope characteristic of a simple diffusion model and the width functions

for a perfect gas. Generally, the shapes of the various $\rho(t)$ are the same for each temperature. In none of the cases is $\rho(t)$ independent of α for $t \gtrsim 1 \times 10^{-13}$ sec, so that in this time range, the Gaussian assumption does not hold exactly. At a given time, the experimental $\rho(t)$ values drop by a factor of about 2 in the α range covered. For times less than 1×10^{-13} sec, the curves agree well and follow the gas behavior expected for very short times. The apparent large differences in the $\rho(t)$'s for $t \lesssim 0.1 \times 10^{-13}$ sec are due to the use of the logarithmic ordinate; on a linear plot these portions of the curves fall very close to each other and the average value of $\rho(0)$ is $\rho(0) \cong \hbar^2 / 2Mk_B T$. At larger times ($t > 1 \times 10^{-13}$ sec.), the slopes of the $\rho(t)$ curves are in all cases much less than that of the simple diffusion model. Assuming that the experimental $\rho(t)$ behavior is ap-

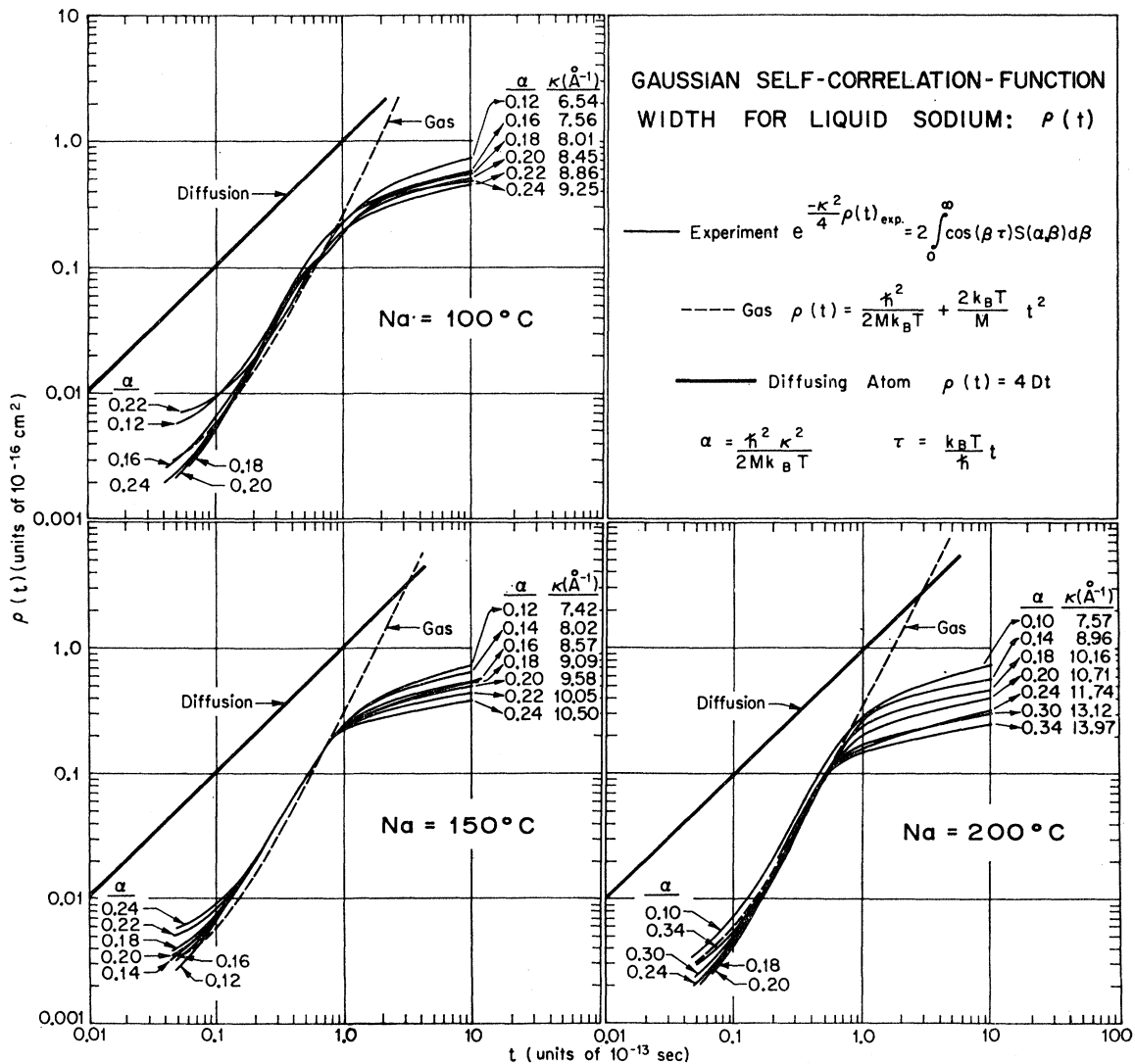


FIG. 11. Time-dependent width functions for sodium, obtained by Fourier transformation of the scattering law assuming a Gaussian form for the self-correlation function.

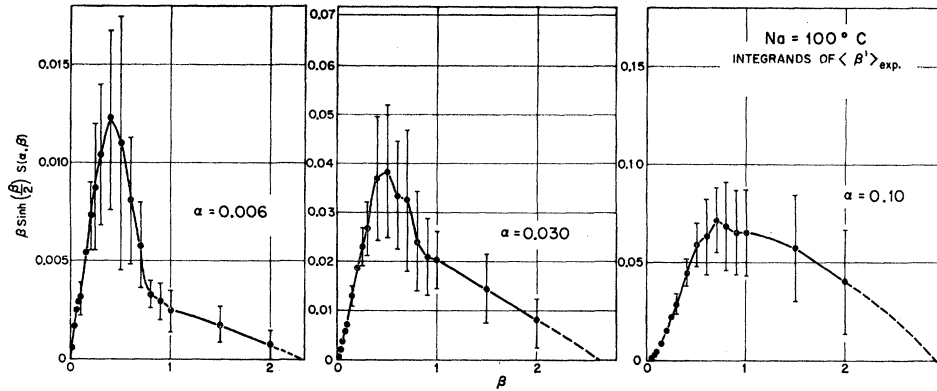


FIG. 12. Representative integrands of the first energy transfer moment of the scattering law for sodium at 100°C.

proximately Gaussian, and that at sufficiently long times it should be proportional to t , characteristic of simple diffusion, it is seen that in the time range available, such diffusive behavior has not yet occurred. The flatness of the curves indicates that for $t < 10 \times 10^{-13}$ sec, the behavior is more nearly that characteristic of a solid. Taking $\rho(t) = 0.5 \times 10^{-16}$ cm² at $t = 10 \times 10^{-13}$ sec then the rms value of r obtained assuming Eq. (3) is 0.87 Å. The nearest neighbor distance r_0 is 3.83 Å so that at such a time the atom is still within the cage of its nearest neighbors and diffusive behavior is not expected. On the other hand at $t \cong 0.8 \times 10^{-13}$, the end of the region of gas-like behavior, $\rho(t) = 2 \times 10^{-16}$ cm² and the rms radius is $r = 0.55$ Å. Thus, the sodium atoms move as free particles for only 15% of the nearest neighbor distance before feeling the effects of binding.

V. MOMENTS OF THE SCATTERING LAW

The results obtained in this experiment have also been used to obtain the first two moments of the energy transfer with respect to the scattering law.¹⁴ Theoretical expressions for these moments were first obtained by Placzek¹⁵ and have been discussed for classical systems by DeGennes.¹⁶ Rahman *et al.*,¹³ have recently rederived the moment relations for the quantum case in a very clear and concise fashion.

Letting $\langle \beta^0 \rangle$ be the zeroth and $\langle \beta^1 \rangle$ the first, then the two lowest energy moments are given in terms of the symmetric scattering law by

$$\langle \beta^0 \rangle \equiv 2 \int_0^\infty \cosh\left(\frac{1}{2}\beta\right) S(\alpha, \beta) d\beta \\ = (1/\sigma_b) \{ \sigma_{inc} + \sigma_{coh} [1 + \gamma(\kappa)] \}, \quad (5)$$

$$\langle \beta^1 \rangle \equiv 2 \int_0^\infty \beta \sinh\left(\frac{1}{2}\beta\right) S(\alpha, \beta) d\beta = \alpha, \quad (6)$$

¹⁴ A brief report on the results of this section has been given in *Phys. Letters* **3**, 162 (1963).

¹⁵ G. Placzek, *Phys. Rev.* **86**, 377 (1952).

¹⁶ P. D. deGennes, *Physica* **25**, 825 (1959).

where σ_b , σ_{inc} and σ_{coh} are the total bound, incoherent, and coherent scattering cross sections, respectively, and $1 + \gamma(\kappa)$ is the structure factor for the liquid. These relations include the effects of both coherent and incoherent scattering. The integrations are to be performed at constant momentum transfer (i.e., constant α) rather than for a fixed scattering angle. Equation (5) is essentially a statement that the integration of the double differential cross section over outgoing energies for fixed momentum transfer is proportional to the diffraction pattern. Equation (6) is a sum rule, the longitudinal f -sum rule which is well known in other aspects of the many-body problem. It is rigorously correct for systems which are reflection invariant and for which the interactions between particles of the system are velocity-independent.¹⁷ Roughly speaking, it states that the mean energy transferred by the neutron is equal to the translational recoil kinetic energy of the scatterer.

The integrations in Eq. (5) and (6) were performed, using a planimeter, for several fixed values of momentum transfer in the range $0.004 \leq \alpha \leq 0.2$ at each temperature. Figure 12 shows some representative integrands of $\langle \beta^1 \rangle$ at the middle and the extremes of the range of $\log \alpha$. The values of $S(\alpha, \beta)$ were taken from the normalized smooth scattering law curves of Figs. 8–10. The error flags on the plotted points were estimated at each β by using the lower limit of the spread of the $S(\alpha, \beta)$ data points of Figs. 6–8. The curve drawn through the points indicates the area of intergration. In all cases beyond $\beta = 2$, the integrand was extrapolated to zero in the manner shown.

The results of the moment measurements for each temperature are shown in Fig. 13. These are shown as the ratio of the observed experimental moments to calculated value at the various values of α . The theoretical zeroth-moment ratios [the right-hand side of Eq. (5)] at all three temperatures were calculated using for $1 + \gamma(\kappa)$ the experimental diffraction results

¹⁷ D. Pines, in *The Many Body Problem*, edited by D. Pines (W. A. Benjamin Inc., New York, 1961), p. 39.

TABLE II. Ratio of observed-to-theoretical moments of the energy transfer.

Temperature	100°C	150°C	200°C
$[\langle \beta^0 \rangle_{\text{obs}} / \langle \beta^0 \rangle_{\text{theor}}]_{\text{av}}$	1.06	1.14	1.11
$[\langle \beta^1 \rangle_{\text{obs}} / \alpha]_{\text{av}}$	2.76 2.30 ^a	2.25 1.82 ^a	1.66 1.42 ^a
$[\langle \beta^1 \rangle_{\text{obs}} / \alpha]_{\text{max}}$	2.05 2.64 ^a	2.75 2.22 ^a	1.92 1.80 ^a

^a Values corrected for multiple scattering.

of Gingrich and Heaton⁷ at 100°C. The results for the zeroth-moment ratios cluster near the value 1 in agreement with Eq. (5). The measured first moments, however, are in marked disagreement with the expected values, being as much as a factor 3 larger than the calculated value. In addition, the discrepancy is temperature-dependent being largest at the lowest temperature. At each temperature, the first-moment ratio also exhibits an apparent α dependence, the ratio decreasing at large and small α . The decrease at large α would be expected since for sufficiently large momentum transfers, the system would act like an ideal gas, and hence, would obey the sum rule. Also, the experimental trend indicates that for α sufficiently small, the sum rule may also be obeyed. In Table II are shown the mean values of the moment ratios plotted in Fig. 13. Also shown are the maximum values of the first moment ratio.

The errors on the first-moment ratio values in Fig. 13 are estimated to be $\pm 35\%$ as obtained from the spread in the scattering-law data points at the various beta values. It is seen that even on the low-limit side of the errors, the first-moment ratios would still disagree with the predicted values. The two major sources of systematic error which could lead to high values of $\langle \beta^1 \rangle_{\text{obs}}$ are the finite energy resolution of the velocity selector and multiple inelastic scattering in the target. Qualitative corrections for finite resolution, which were made when drawing the scattering law, were checked at 100°C by convoluting the known velocity-selector burst shape with the partial differential cross section regenerated from this smooth-curve scattering law at the smallest scattering angle (16.3°) and the highest incident energy (0.1 eV), where resolution effects are the largest. The resulting cross section agrees within $\pm 10\%$ with data for that angle. Also, the effects of energy resolution are in general most pronounced for the smallest energy transfers ($\beta \leq 0.2$), and this region contributes little to the first moment integral (see Fig. 12). In any case, at large scattering angles (large alpha) where the cross section peaks are broad compared with the burst width, energy resolution effects would be small.

Since the target is thin, scattering only 8% of the incident beam, multiple scattering effects should be small. In order to determine to what extent multiple scattering affects the first moment, an estimate of the multiple scattering was made by fitting $S(\alpha, \beta)$ to a polynomial in α and assuming that the zeroth-order

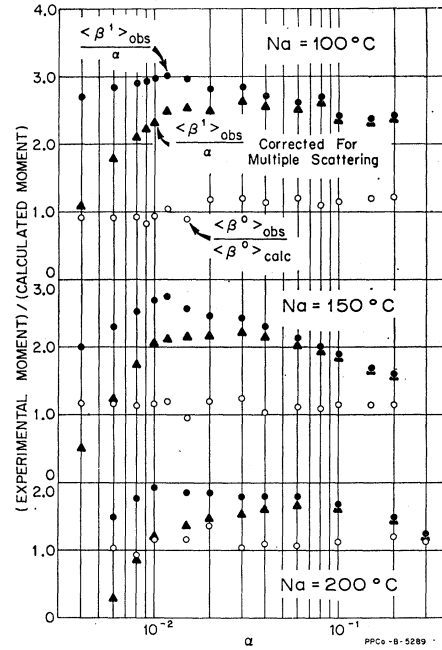


FIG. 13. Ratios of the observed to the calculated zeroth and first energy transfer moments of the scattering law for sodium at 100, 150 and 200°C.

term arises from multiple scattering,¹ i.e.,

$$S(\alpha, \beta) = A_0(\beta) + A_1(\beta)\alpha + A_2(\beta)\alpha^2 + A_3(\beta)\alpha^3 + \dots$$

Since the first term in a theoretical expression of $S(\alpha, \beta)$ is proportional to α and since multiple scattering is expected to be roughly isotropic and hence independent of α , it is assumed that the term $A_0(\beta)$ is due to multiple scattering. The first moment ratio, corrected for multiple scattering is then given by

$$\langle \beta^1 \rangle_{\text{corr}} / \alpha = (\langle \beta^1 \rangle_{\text{obs}} / \alpha) - (A_0(\beta) / \alpha),$$

where the correction term $\langle \beta^1 \rangle$ is obtained from the same integral as Eq. (6) with $S(\alpha, \beta)$ replaced by $A_0(\beta)$. This correction is not expected to be exact, but the procedure is a reasonable one and is the best practical one available at the present time. Its accuracy is unknown and cannot be determined until experimental measurements of multiple inelastic scattering are available.

The $S(\alpha, \beta)$ curves of Figs. 8-10 for $\beta \geq 0.25$ were least-squares fit to a third-order polynomial in α in order to obtain $A_0(\beta)$. Scattering-law values for $\beta < 0.25$ were not used since the extrema in $S(\alpha, \beta)$ caused by coherent scattering would necessitate a much higher order polynomial. The values of $A_0(\beta)$ for $\beta < 0.25$ were obtained by extrapolating $A_0(\beta)$ to $\beta = 0$. Table III shows the amount of multiple scattering compared to the peak value of $S(\alpha, \beta)$, i.e., $A_0(0) / S(\alpha, 0)$ at each temperature together with the value of $\langle \beta^1 \rangle$, the correction to the observed first moment. Table II gives

TABLE III. Multiple scattering correction to the observed first energy transfer moment.

Temperature °C	100	150	200
$A_0(0)/S(\alpha,0)$	0.027	0.059	0.092
$\langle\beta_e^2\rangle$	0.0064	0.0063	0.0072

the values of the average and maximum of the first-moment ratio, corrected for multiple scattering. The resulting first-moment ratios corrected for multiple scattering are shown in Fig. 13. Since the correction to the first-moment ratio is proportional to α^{-1} , the largest effect occurs at small α . At small α the correction is large and accounts for most of the measured ratio and may be an over correction. At large momentum transfers the correction becomes negligible. In general, for $\alpha \gtrsim 0.010$ at all temperatures the corrected moments are still much larger than predicted theoretically. A conceivable explanation for this is that velocity-dependent interactions might be important in the liquid or else that reflection invariance does not hold. However, it is extremely unlikely that reflection invariance would fail in a monatomic liquid. Also there is little reason to expect, nor is there other evidence to support the hypothesis that velocity-dependent interactions play any great role in a liquid. Additional scattering experiments of higher precision would be needed to make such hypotheses tenable.

SUMMARY AND CONCLUSIONS

The scattering law for liquid sodium between 100 and 200°C has been measured in the range of momentum transfer $1 \lesssim \kappa \lesssim 10 \text{ \AA}^{-1}$ for energy transfers out to about

0.06 eV. The scattering law shows pronounced maxima due to inelastic coherent scattering for energy transfers below $0.2 k_B T$, but which disappear for larger energy transfer, demonstrating that the convolution approximation does not hold in general for liquid Na. Time-dependent Gaussian width functions obtained by Fourier transformation of the scattering law at several momentum transfers show that sodium behaves as an ideal gas for times less than 1.0×10^{-13} sec corresponding to an rms atomic displacement of 15% of the nearest neighbor distance, but for larger times behaves more like a solid. In the time range available, $\lesssim 10 \times 10^{-13}$ sec, there is no evidence that simple diffusive behavior has been approached. The width functions for times greater than 1×10^{-13} sec are momentum-dependent, showing that the Gaussian assumption for the self-correlation function does not hold rigorously for momentum transfers larger than $K \approx 6 \text{ \AA}^{-1}$. Measurements of the two lowest moments of the energy transfer show that the zeroth moment gives the expected results but that the first moment is much larger than the theoretical values for a wide range of momentum transfers. The cause of this discrepancy remains to be explained. Whatever the underlying physical reasons for the discrepancy, it should not be peculiar to sodium, but should also appear in other metals. In any case, it would be of interest if energy transfer moments were measured in other metallic liquids.

ACKNOWLEDGMENTS

The author is much indebted to Dr. G. W. Griffing and G. Marshall for many helpful discussions, and to Dr. R. M. Brugger and Dr. R. G. Fluharty for advice and encouragement during this experiment.